

# Activation Energy and Mechanism of the Molybdenum Disilicide Sintering Process

D. D. Titov<sup>a,\*</sup>, Yu. F. Kargin<sup>a</sup>, A. S. Lysenkov<sup>a</sup>, P. A. Miloserdov<sup>b</sup>, S. N. Perevislov<sup>c</sup>, N. V. Petrakova<sup>a</sup>, O. S. Antonova<sup>a</sup>, A. A. Konovalov<sup>a</sup>, A. A. Ashmarin<sup>a</sup>, and A. V. Shokod'ko<sup>a</sup>

<sup>a</sup>Baikov Institute of Metallurgy and Materials Science, Russian Academy of Sciences, Leninskii pr. 49, Moscow, 119334 Russia

<sup>b</sup>Merzhanov Institute of Structural Macrokinetics and Materials Science, Russian Academy of Sciences, ul. Akademika Osip'yana 8, Chernogolovka, Moscow oblast, 142432 Russia

<sup>c</sup>St. Petersburg State Technological Institute (Technical University), Moskovskii pr. 24–26/49, St. Petersburg, 190013 Russia

\*e-mail: mitytitov@gmail.com

Received April 9, 2018

**Abstract**—This paper presents dilatometric analysis data for the sintering of off-the-shelf molybdenum disilicide ( $\text{MoSi}_2$ ) powder prepared by magnesiothermic synthesis. We have obtained continuous shrinkage curves for  $\text{MoSi}_2$  powder compacts with an initial relative density of 70% at different heating rates: 5, 10, 20, and 30°C/min. From a quantitative analysis of densification curves for the compacts, the activation energy for the initial stage of sintering has been determined to be  $Q = 695$  kJ/mol. It has been shown that the dominant process in the initial stage of  $\text{MoSi}_2$  powder sintering is volume diffusion from grain boundaries and surfaces.

**Keywords:** molybdenum disilicide,  $\text{MoSi}_2$ , dilatometry, activation energy, sintering mechanism

**DOI:** 10.1134/S0020168518110134

## INTRODUCTION

Molybdenum disilicide ( $\text{MoSi}_2$ ,  $\rho = 6.23$  g/cm<sup>3</sup>) has low resistivity ( $\sigma = 21$   $\mu\Omega$ /cm<sup>2</sup>) [1] and the highest oxidation resistance at temperatures above 1000°C among all disilicides. The high oxidation resistance of  $\text{MoSi}_2$  is due to the formation of a protective surface silicon oxide film, which prevents oxygen indiffusion and further oxidation of the material. Owing to this, molybdenum disilicide and  $\text{MoSi}_2$ -based materials are widely used as heating elements of furnaces working in air. Attempts to use pure  $\text{MoSi}_2$  as structural ceramics (for example, for the fabrication of turbine blades) have had limited success [2] because of its brittleness at room temperature, creep at high temperatures, and low oxidation resistance in the temperature range 500–800°C, where molybdenum disilicide suffers from “catastrophic” oxidation [3] and undergoes complete destruction to give the  $\text{MoO}_3$  and  $\text{SiO}_2$  oxides [4].

Despite intense studies of  $\text{MoSi}_2$ -based materials, neither the mechanism nor the activation energy of the molybdenum disilicide sintering process has been reported to date. Knowledge of the sintering mechanism and related parameters, such as the activation energy for sintering, are helpful [5] in optimizing processes underlying the fabrication of desired parts with tailored densification and microstructure.

The purpose of this work was to study the  $\text{MoSi}_2$  sintering process and evaluate its activation energy.

## EXPERIMENTAL

**Starting materials.** In our preparations, we used off-the-shelf high-purity (99.5%)  $\text{MoSi}_2$  powder prepared by magnesiothermic synthesis (OOO Plasmatorm, Moscow) and characterized by scanning electron microscopy (SEM), X-ray diffraction, and particle size analysis. Figure 1 shows an SEM image of  $\text{MoSi}_2$  powder particles (Supra 50 VP LEO scanning electron microscope equipped with an Oxford Instruments INCA Energy+ X-ray microanalysis system (Germany)). It is seen that the powder particles range widely in shape (polyhedral) and size, and that there are agglomerates of smaller particles between large particles. The particle size distribution of the powder was determined using an Analysette 22 laser particle sizer (Fritsch, Germany). The distribution was found to have three broad maxima in the range 0.5–60  $\mu\text{m}$ , with average particle sizes of 3, 10 (predominant size fraction), and 40  $\mu\text{m}$ .

According to X-ray diffraction data, the polycrystalline  $\text{MoSi}_2$  powders were single-phase, with a trace amount of  $\text{Mo}_5\text{Si}_3$  (within 0.5%) as an impurity phase.

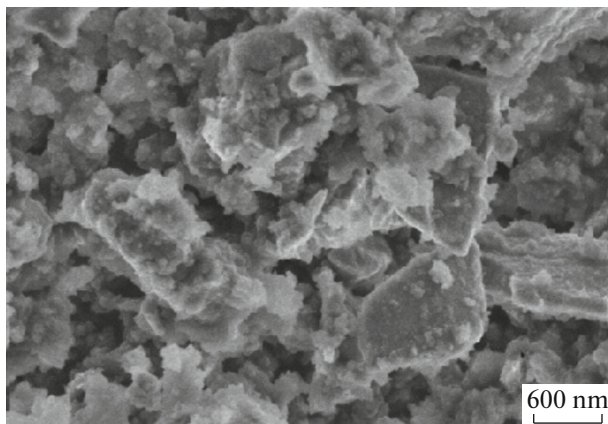


Fig. 1. SEM image of the starting MoSi<sub>2</sub> powder.

**Sample preparation.** The powders were uniaxially pressed into disks 5 mm in diameter and ~2.5 mm in thickness in a metallic press die set at room temperature on a hydraulic press at a pressure of 400 MPa. The weight of each sample was 0.2 g. The samples were weighed on an analytical balance with an accuracy of 0.001 g and their relative density was evaluated from their mass and geometric dimensions. In dilatometric characterization, we used samples identical in initial relative density (70.0%).

**Dilatometric analysis.** Dilatometric data were obtained on a DIL 402C dilatometer (Netzsch, Germany) [6]. A sample was placed in a horizontal corundum holder fitted with a corundum pushrod and precision displacement transducer (measuring range from 500 to 5000 μm). To more accurately monitor the temperature, a platinum thermocouple (type B) was placed in the immediate vicinity of the sample. Argon was introduced into the furnace at a flow rate of 70 mL/min. The heating rate was 5, 10, 20, or 30°C/min. The samples were heated to a temperature of 1450°C and then cooled to room temperature at a rate of 20°C/min.

Under the assumption that the sample densification process was isotropic, the relative density of the sintered sample ( $\rho_s$ ) was evaluated using the following equation [5, 7];

$$\rho_s = \left[ \frac{1}{1 + \frac{\Delta L}{L_0} - \alpha(T - T_0)} \right]^3 \rho_g, \quad (1)$$

where  $\Delta L/L_0$  is the relative linear shrinkage evaluated by dilatometry,  $L_0$  is the initial sample length,  $T$  is the measured temperature,  $T_0$  is the initial temperature,  $\rho_g$  is the green density, and  $\alpha$  is the linear thermal expansion coefficient (LTEC). The LTEC of the samples was determined in the cooling stage of dilatometric

analysis [8, 9]. The average  $\alpha$  was determined using cooling curves of the samples (that is, after sintering at different heating rates).

After dilatometric analysis, the density of the samples was determined by saturating the body with liquid, followed by hydrostatic weighing (Russian Federation State Standard GOST 7025-91). Distilled water was used as a suspending medium.

## RESULTS AND DISCUSSION

The derivation of initial sintering equations can be found in Refs. [10–14]. Young and Cutler [15] obtained equations for the sintering rate, which are applicable to a quantitative analysis of shrinkage parameters measured at a constant heating rate (CHR) [5] and evaluated the activation energy for the firing process in the initial stage of sintering. Wang and Raj [16, 17] obtained an equation for the sintering rate which is used to estimate the activation energy for the intermediate stage of sintering by the CHR method. To identify the initial sintering mechanism using the CHR approach, Matsui et al. [18, 19] proposed a useful combination of equations derived by Young and Cutler [15] and Wang and Raj [16, 17]. The procedure was successfully applied in studies of the effect of SiO<sub>2</sub> [20], Al<sub>2</sub>O<sub>3</sub> [18, 19, 21], GeO<sub>2</sub> [22], and Y<sub>2</sub>O<sub>3</sub> [23] on the initial sintering of zirconia powder and the sintering kinetics of ThO<sub>2</sub> + 4% UO<sub>2</sub> granules [24].

Matsui et al. [18, 19] obtained two equations for sintering at a constant heating rate:

$$\ln \left[ TC \frac{dp}{dT} \right] = -\frac{Q}{RT} + \ln [f(\rho)] + \ln \left[ \frac{K\gamma\Omega D_0}{k_B} \right] - p \ln a, \quad (2)$$

$$\frac{d \left( \frac{\Delta L}{L_0} \right)}{dT} = \ln \left( \frac{K\gamma\Omega D_0 R}{k_B a^p C Q} \right)^n \exp \left( \frac{nQ}{RT^{2-n}} \right) \exp \left( -\frac{nQ}{RT} \right), \quad (3)$$

where  $T$  is the absolute temperature,  $C$  is the heating rate,  $dp/dT$  is the densification rate,  $Q$  is the activation energy,  $R$  is the gas constant,  $f(\rho)$  is a function of density,  $K$  is a numerical constant,  $\gamma$  is the surface energy,  $\Omega$  is the atomic volume,  $D_0$  is the frequency coefficient,  $k_B$  is Boltzmann's constant,  $a$  is the particle radius,  $\Delta L = L_0 - L$  is the change in the length of the compacts,  $L_0$  is the initial length of the compacts, and the parameters  $n$  and  $p$  depend on the diffusion mechanism. Equations (2) and (3) are applicable at shrinkages below 4%.

To identify the mechanism operative in the initial stage of MoSi<sub>2</sub> sintering, the input dilatometric data

obtained at a constant heating rate were plotted as follows: Using Eq. (2), we found the slope  $S_1$  of the plot of  $\ln \left[ TC \frac{d\rho}{dT} \right]$  against  $1/T$  at constant density and determined the activation energy using the relation

$$Q = -RS_1. \quad (4)$$

Using Eq. (3) and the slope  $S_2$  of the plot of  $\ln \left[ T \frac{d \left( \frac{\Delta L}{L_0} \right)}{dT} \right]$  against  $1/T$ , we determined the apparent activation energy as

$$nQ = -RS_2. \quad (5)$$

Combining Eqs. (5) and (6), we obtain the parameter  $n$ , which characterizes the initial sintering mechanism:

$$n = \frac{nQ}{Q} = \frac{S_2}{S_1}. \quad (6)$$

Figures 2 and 3 show the variation of the shrinkage and shrinkage rate for the  $\text{MoSi}_2$  samples during non-isothermal sintering at four different heating rates: 5, 10, 20, and  $30^\circ\text{C}/\text{min}$ . At each heating rate, we observe regions of normal linear expansion of molybdenum disilicide and then (above the shrinkage onset temperature) a shrinkage process. The sintering results are compared in Table 1.

The dilatometric analysis data demonstrate that, with increasing heating rate, the sintering onset temperature shifts to higher temperatures:  $t_{\text{shrinkage onset}} = 1189.9^\circ\text{C}$  at  $5^\circ\text{C}/\text{min}$  and  $1232.6^\circ\text{C}$  at  $30^\circ\text{C}/\text{min}$ . This behavior is related mainly to the kinetics of the process and was observed previously for the sintering of  $\text{ZrO}_2$  [22],  $\text{Li}_2\text{TiO}_3$  [5], and  $(\text{Mo,W})\text{Si}_2 + \text{Si}_3\text{N}_4$  [4]. It can be interpreted as follows: at a lower heating rate, the sample expands for a longer time before shrinkage onset and shrinks for a longer time before a particular temperature is reached [25]. For the same reason, the shrinkage rate curves of the samples were observed to shift to higher temperatures with increasing heating rate. The maximum shrinkage rate was found to depend on the heating rate: the higher the heating rate, the higher the instantaneous shrinkage rate, independent of temperature. Such behavior is well documented and was reported previously for  $\text{Al}_2\text{O}_3$  [26] and 3Y-TZP [7].

Using Eq. (1), the experimental continuous shrinkage curves (Fig. 2) were represented as plots of the relative density (percent of the theoretical density) against temperature. The temperature dependences of relative density for the  $\text{MoSi}_2$  samples are presented in Fig. 4. With increasing heating rate, the curves shift to

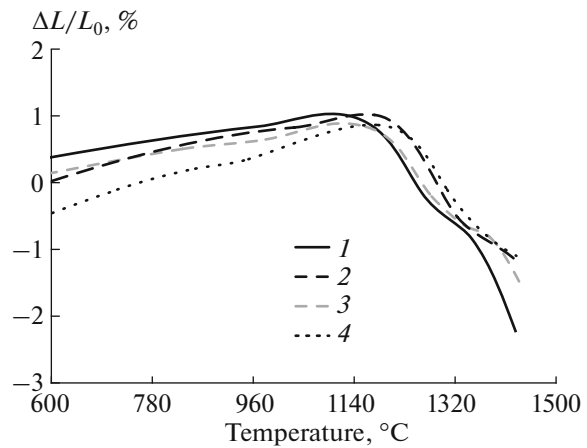


Fig. 2. Effect of heating rate on the  $\text{MoSi}_2$  sintering process: (1) 5, (2) 10, (3) 20, and (4)  $30^\circ\text{C}/\text{min}$ .

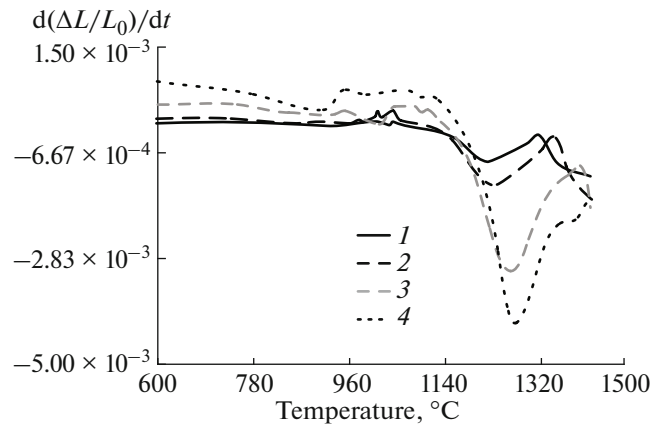
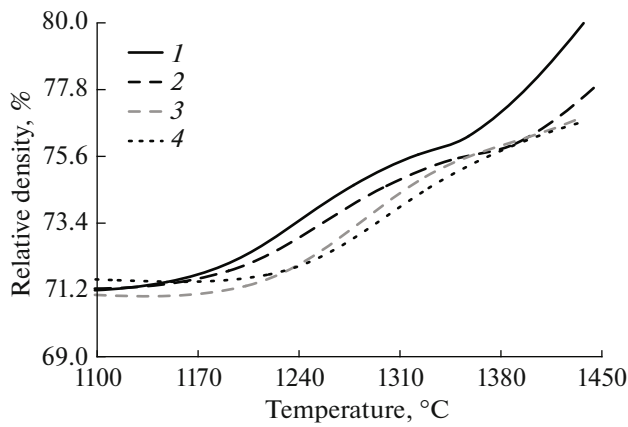


Fig. 3. Effect of heating rate on the  $\text{MoSi}_2$  shrinkage rate: (1)–(4) same as in Fig. 2.

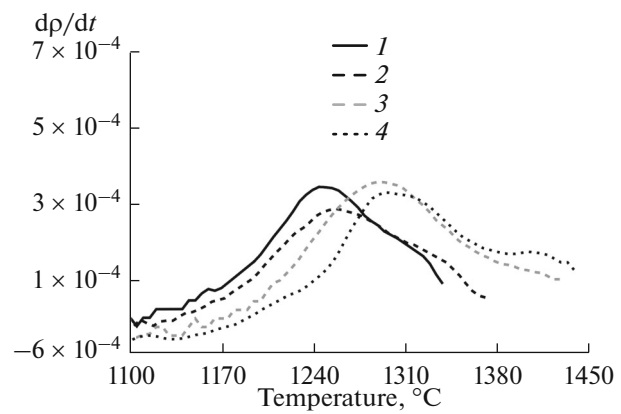
higher temperatures. It is worth noting that, throughout the temperature range examined, the density reached by sintering varied moderately but systematically with heating rate. The maximum density was shown to depend on heating rate: the higher the heating rate, the lower the density of the sintered material. Such behavior was reported previously for zirconia [8], alumina [26], ceria [27], magnesium aluminate [28], and  $\text{Li}_2\text{TiO}_3$  [5] and is consistent with the fact that, at a slower heating rate, a green compact is sintered for a

Table 1. Dilatometric analysis data for  $\text{MoSi}_2$

Heating rate, $^\circ\text{C}/\text{min}$	$t_{\text{shrinkage onset}}, ^\circ\text{C}$	$t_{\text{max}}, ^\circ\text{C}$
5	1189.9	1239
10	1195.5	1247
20	1225.3	1283
30	1232.6	1305



**Fig. 4.** Relative density of MoSi<sub>2</sub> as a function of temperature during nonisothermal sintering at different heating rates: (1)–(4) same as in Fig. 2.



**Fig. 5.** Densification rate as a function of temperature for MoSi<sub>2</sub> at different heating rates: (1)–(4) same as in Fig. 2.

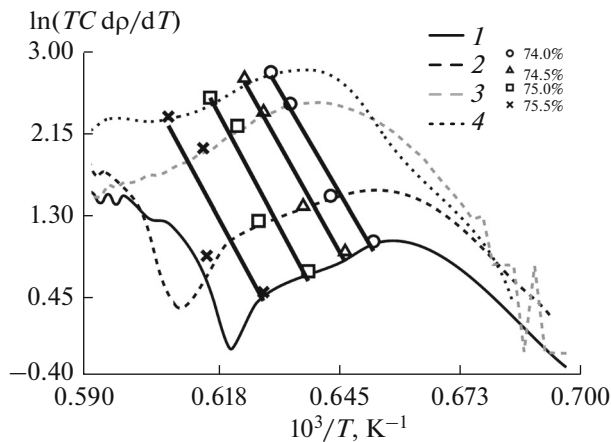


**Fig. 6.** Plots of ln(TC dp/dT) against 1/T for MoSi<sub>2</sub> at different heating rates: (1)–(4) same as in Fig. 2.

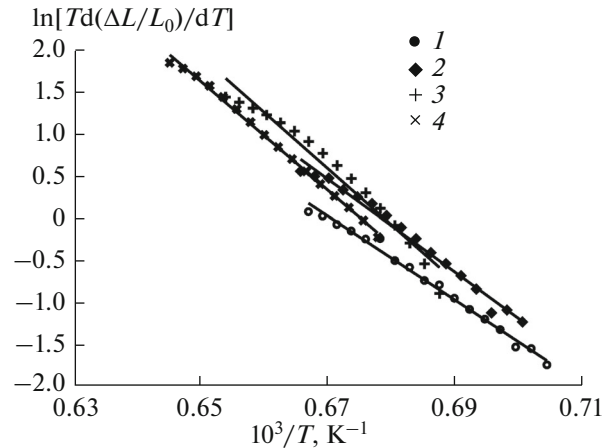


**Fig. 7.** Plots of ln[Td(ΔL/L<sub>0</sub>)/dT] against 1/T for MoSi<sub>2</sub> at different heating rates: (1)–(4) same as in Fig. 2.

longer time and, accordingly, the resultant shrinkage is higher.

Figure 5 shows the densification rate ( $dp/dt$ ) as a function of temperature for MoSi<sub>2</sub> at heating rates from 5 to 30°C/min. With increasing heating rate, the peaks shift to higher temperatures, but their height remains almost unchanged. According to Wang and Raj [16], higher peak temperatures and heights are indicative of a higher activation energy.

The activation energy ( $Q$ ) and apparent activation energy ( $nQ$ ) of initial MoSi<sub>2</sub> sintering and the order  $n$

related to the sintering mechanism were evaluated using formulas (2), (3), and (6). For each heating rate, we determined the temperature  $t$  and heating rate  $dt/d\tau = C$  at the same relative density of the samples. The data thus obtained were represented as plots of  $\ln[TC(dp/dT)]$  against  $1/T$  (Fig. 6). The calculations were performed for relative densities under 76%, which corresponded to shrinkages under 4%. It is seen that the plots for each relative density of the samples are linear. The activation energy ( $Q$ ) of the sintering process at each relative density was determined from the slope of the cor-

**Table 2.** Activation energy, apparent activation energy, and order related to the diffusion mechanism in the initial stage of MoSi<sub>2</sub> sintering.

$n$	$Q$	Standard deviation	$nQ$	Standard deviation
0.70	695	27	487	66

responding straight line. The results are presented in Table 2. The average activation energy is 695 kJ/mol.

The apparent activation energy ( $nQ$ ) was determined for each heating rate using Eq. (3) in the shrinkage range <4% from the slope of the straight line obtained by plotting  $\ln[Td(\Delta L/L_0)/dT]$  against  $1/T$  (Fig. 7). At all heating rates from 5 to 30°C/min, we obtained linear plots. The average  $nQ$  is 487 kJ/mol (Table 2). The value of  $n$  was determined using formula (6) and the average  $Q$  and  $nQ$  (Table 2).

According to a model for the sintering of two spherical particles, the values  $n = 0.31$ – $0.33$  correspond to grain-boundary diffusion,  $n = 0.40$ – $0.50$  corresponds to volume diffusion only from grain boundaries, and  $n > 0.53$  corresponds to volume diffusion from a grain boundary and the surface of the spheres [12]. Comparison of the  $n = 0.70$  obtained in this study with the above model values leads us to conclude that the most likely MoSi<sub>2</sub> sintering mechanism is volume diffusion from grain boundaries and the surface of the particles.

## CONCLUSIONS

We have obtained continuous shrinkage curves for MoSi<sub>2</sub> powder compacts with an initial relative density of 70% at different heating rates: 5, 10, 20, and 30°C/min. It has been shown that the dominant mechanism controlling MoSi<sub>2</sub> densification in the initial stage of sintering is volume diffusion from grain boundaries and the surface of the particles, with an activation energy  $Q = 695$  kJ/mol.

## ACKNOWLEDGMENTS

This work was supported by the Russian Foundation for Basic Research, grant no. Mol\_a 18-38-00327. The experimental work (X-ray diffraction, scanning electron microscopy, and particle size analysis) was supported by the Russian Federation Ministry of Science and Higher Education (state research target no. 007-00129-18-00). We are grateful to our colleagues at OOO Plazmoterm for supplying the raw materials and for fruitful discussions.

## REFERENCES

- Samsonov, G.V., Dvorina, L.A., and Rud', B.M., *Silit-sidy* (Silicides), Moscow: Metallurgiya, 1979, p. 271.
- Gladyshevskii, E.I., *Kristalokhimiya silit-sidov i germanidov* (Crystal Chemistry of Silicides and Germanides), Moscow: Metallurgiya, 1971, p. 156.
- Melsheimer, S., Oxidation of the intermetallics MoSi<sub>2</sub> and TiSi<sub>2</sub>, *Comparison*, 1997, vol. 47, nos. 1–2, pp. 139–203.
- Titov, D.D., Lysenkov, A.S., Kargin, Y.F., Gorshkov, V.A., Goldberg, M.A., and Petrakova, N.V., Low-temperature oxidation of MoSi<sub>2</sub>–Si<sub>3</sub>N<sub>4</sub> composites, *Inorg. Mater.: Appl. Res.*, 2016, vol. 7, no. 4, pp. 624–629.
- Abbasian, A.R., Rahimpour, M.R., and Hamnabard, Z., Initial sintering kinetics of lithium meta titanate at constant rates of heating, *Iranian J. Mater. Sci. Eng.*, 2013, vol. 10, no. 3, pp. 44–53.
- Trusova, E.A., Khrushchev, A.A., Vokhmintcev, K.V., and Titov, D.D., Dilatometric sintering study of fine-grained ceramics from ultradispersed admixture composed of Ce<sub>0.09</sub>Zr<sub>0.91</sub>O<sub>2</sub> and MgO–Al<sub>2</sub>O<sub>3</sub>, *J. Eur. Ceram. Soc.*, 2013, vol. 33, no. 12, pp. 2327–2333.
- Mazaheri, M., Simchi, A., Dourandish, M., and Golestani-Fard, F., Master sintering curves of a nanoscale 3Y-TZP powder compacts, *Ceram. Int.*, 2009, vol. 35, no. 2, pp. 547–554.
- Bernard-Granger, G. and Guizard, C., Apparent activation energy for the densification of a commercially available granulated zirconia powder, *J. Am. Ceram. Soc.*, 2007, vol. 90, no. 4, pp. 1246–1250.
- Chen, L., Dilatometric analysis of sintering of tungsten and tungsten with ceria and hafnia dispersions, *Refract. Met. Hard Mater.*, 1993, vol. 12, no. 1, pp. 41–51.
- Kingery, W.D. and Berg, M., Study of the initial stages of sintering solids by viscous flow, evaporation–condensation, and self-diffusion, *J. Appl. Phys.*, 1955, vol. 26, no. 10, pp. 1205–1212.
- Coble, R.L., Initial sintering of alumina and hematite, *J. Am. Ceram. Soc.*, 1958, vol. 41, no. 2, pp. 55–62.
- Johnson, D.L. and Cutler, I.B., Diffusion sintering: initial stage sintering models and their application to shrinkage of powder compacts, *J. Am. Ceram. Soc.*, 1963, vol. 46, no. 11, pp. 541–545.
- Geguzin, Ya.E., *Fizika spekaniya* (The Physics of Sintering), Moscow: Nauka, 1967, p. 360.
- Bakunov, V.S., Belyakov, A.V., Lukin, E.S., and Shayakhmetov, U.Sh., *Oksidnaya keramika: spekanie i polzuechest'* (Oxide Ceramics: Sintering and Creep), Moscow: Ross. Khim. Tekhnol. Univ. im. D.I. Mendeleeva, 2007, p. 584.
- Young, W.S. and Cutler, I.B., Initial sintering with constant rates of heating, *J. Am. Ceram. Soc.*, 1970, vol. 53, no. 12, pp. 659–663.
- Wang, J. and Raj, R., Estimate of the activation energies for boundary diffusion from rate-controlled sintering of pure alumina, and alumina doped with zirconia or titania, *J. Am. Ceram. Soc.*, 1990, vol. 73, no. 5, pp. 1172–1175.
- Wang, J. and Raj, R., Activation energy for the sintering of two-phase alumina/zirconia ceramics, *J. Am. Ceram. Soc.*, 1991, vol. 74, no. 8, pp. 1959–1963.
- Matsui, K., Ohmichi, N., Ohgai, M., Enomoto, N., and Hojo, J., Sintering kinetics at constant rates of heating: effect of Al<sub>2</sub>O<sub>3</sub> on the initial sintering stage of fine zirconia powder, *J. Am. Ceram. Soc.*, 2005, vol. 88, no. 12, pp. 3346–3352.
- Matsui, K., Tanaka, K., Enomoto, N., and Hojo, J., Sintering kinetics at constant rates of heating: effect of alumina on the initial sintering stage of yttria-stabilized

- cubic zirconia powder, *J. Ceram. Soc. Jpn.*, 2006, vol. 114, no. 1333, pp. 763–768.
20. Matsui, K., Sintering kinetics at constant rates of heating: mechanism of silica-enhanced sintering of fine zirconia powder, *J. Am. Ceram. Soc.*, 2008, vol. 91, no. 8, pp. 2534–2539.
  21. Suárez, G. and Sakka, Y., Effect of alumina addition on initial sintering of cubic  $ZrO_2$  (8YSZ), *Ceram. Int.*, 2010, vol. 36, no. 3, pp. 879–885.
  22. Matsui, K. and Hojo, J., Sintering kinetics at constant rates of heating: effect of  $GeO_2$  addition on the initial sintering stage of 3 mol %  $Y_2O_3$ -doped zirconia powder, *J. Mater. Sci.*, 2008, vol. 43, no. 3, pp. 852–859.
  23. Mazaheri, M., Golestani-Fard, F., and Simchi, A., An investigation on densification of nanocrystalline 3Y-TZP using master sintering curve, *Int. Conf. and Exhibition of the Eur. Ceram. Soc.*, Cádiz, 2012.
  24. Banerjee, J., Kutty, T.R.G., Kumar, A., Kamath, H.S., and Banerjee, S., Densification behaviour and sintering kinetics of  $ThO_2$ -4%  $UO_2$  pellet, *J. Nucl. Mater.*, 2011, vol. 408, no. 3, pp. 224–230.
  25. Sato, E. and Carry, C., Yttria doping and sintering of submicrometer-grained  $\alpha$ -alumina, *J. Am. Ceram. Soc.*, 1996, vol. 79, no. 8, pp. 2156–2160.
  26. Aminzare, M., Golestani-fard, F., Guillon, O., Mazaheri, M., and Rezaie, H.R., Sintering behavior of an ultrafine alumina powder shaped by pressure filtration and dry pressing, *Mater. Sci. Eng., A*, 2010, vol. 527, nos. 16–17, pp. 3807–3812.
  27. Kinemuchi, Y. and Watari, K., Dilatometer analysis of sintering behavior of nano- $CeO_2$  particles, *J. Eur. Ceram. Soc.*, 2008, vol. 28, no. 10, pp. 2019–2024.
  28. Rozenburg, K., Reimanis, I.E., Kleebe, H.J., and Cook, R.L., Sintering kinetics of a  $MgAl_2O_4$  spinel doped with LiF, *J. Am. Ceram. Soc.*, 2008, vol. 91, no. 12, pp. 444–450.

*Translated by O. Tsarev*